THE JOURNAL OF PHYSICAL CHEMISTRY LETTERS
A JOURNAL OF THE AMERICAN CHEMICAL SOCIETY

pubs.acs.org/JPCL

Letter

Long-Range Charge Separation Enabled by Intramoiety Delocalized Excitations in Copolymer Donors in Organic Photovoltaic Blends

Qian Li, Rui Wang, Tao Yu, Xiaoyong Wang, Zhi-Guo Zhang, Yuan Zhang, Min Xiao,* and Chunfeng Zhang*

Cite This: *J. Phys. Chem. Lett.* 2023, 14, 7498−7506

Read Online

ACCESS | Metrics & More | Article Recommendations | Supporting Information

ABSTRACT: For over two decades, most high-performance organic photovoltaics (OPVs) have been made with donor:acceptor bulk heterojunctions with domain sizes limited by exciton diffusion, where charge separation mostly takes place through the dissociation of the interfacial charge-transfer (xCT) excitons. Recently, nonfullerene acceptor (NFA)-based OPVs have shown excellent compatibility to device structures with large domains in active layers. However, it remains elusive how the excitations that are distant from the interfaces are converted into free charges. Here, we report the identification of a new charge separation channel in model copolymer/NFA blends mediated by intra-moiety delocalized excitations in both planar heterojunctions and donor-enriched bulk heterojunctions. The delocalized excitations induced by interchromophore electronic interactions in copolymer donors mediate the long-range charge separation and dissociate into free charges without forming the bound xCT states first, releasing the constraints associated with the short exciton diffusion length in organic materials. The long-range charge separation mechanism uncovered in this work, in cooperation with the short-range xCT-mediated pathway, holds the potential to further optimize OPVs with diverse device structures.

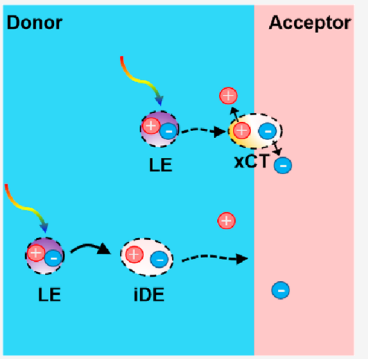

In organic photovoltaic (OPV) devices, it is generally assumed that free charges are generated by the dissociation of charge-transfer (CT) excitons at the interfaces of electron donor and acceptor materials.[1−5] The short exciton diffusion lengths in most OPV materials impose strict limits on the domain sizes of donors and acceptors.[6] This issue is the major reason for the inferior performance of devices using original planar heterojunction (PHJ) structure[7] (Figure 1a) in comparison to the bulk heterojunction (BHJ) structure (Figure 1b).[8] Owing to the trade-off between multiple factors including light absorption, exciton diffusion, charge separation, and transport, optimal power conversion efficiencies (PCEs) for most OPV devices are achieved with active layers as thin as ∼100 nm.[9] Recently, OPV devices with the state-of-the-art nonfullerene acceptors (NFAs) show improved compatibility with thicker device structures. The PCEs are largely retained in the devices using sequentially processed pseudo-PHJ structures[10−19] (Figure 1c) or BHJ structures with active layers much thicker than 100 nm.[19−21] These improvements are of great technical significance for a large scale printing procedure toward commercial applications.[12] Optical excitations in these device structures may be created distantly from the donor:acceptor interface (Figure 1d). It remains elusive how these distant excitations separate into free charges at a high quantum efficiency in the active layers.

In conventional BHJ structures, a large number of excitons are created next to the interface. The scenario of xCT-mediated pathway established in polymer/fullerene blends has been naturally extended in explaining the charge separation

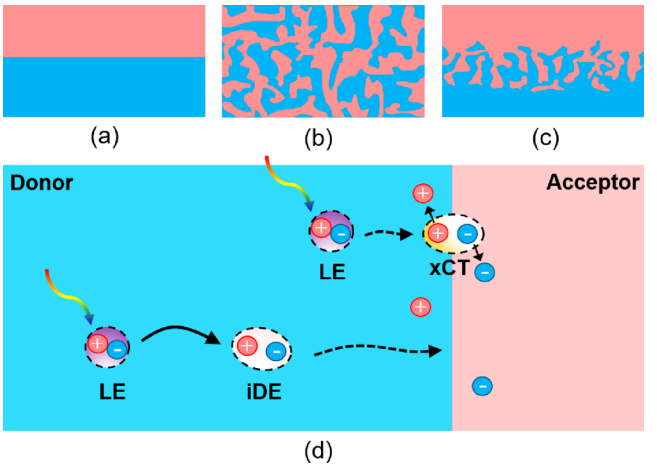

Figure 1. Typical structures of (a) the bilayer planar heterojunction, (b) the bulk heterojunction, and (c) the pseudo-planar heterojunction used in OPV devices. (d) In addition to the direct diffusion from local excitations to the donor:acceptor interface, local excitations created distantly from the donor:acceptor interface may undergo a charge separation channel mediated by intra-moiety delocalized excitations.

Received: July 6, 2023
Accepted: August 11, 2023
Published: August 15, 2023

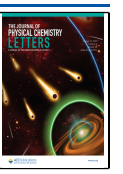

https://doi.org/10.1021/acs.jpclett.3c01861
J. Phys. Chem. Lett. 2023, 14, 7498−7506

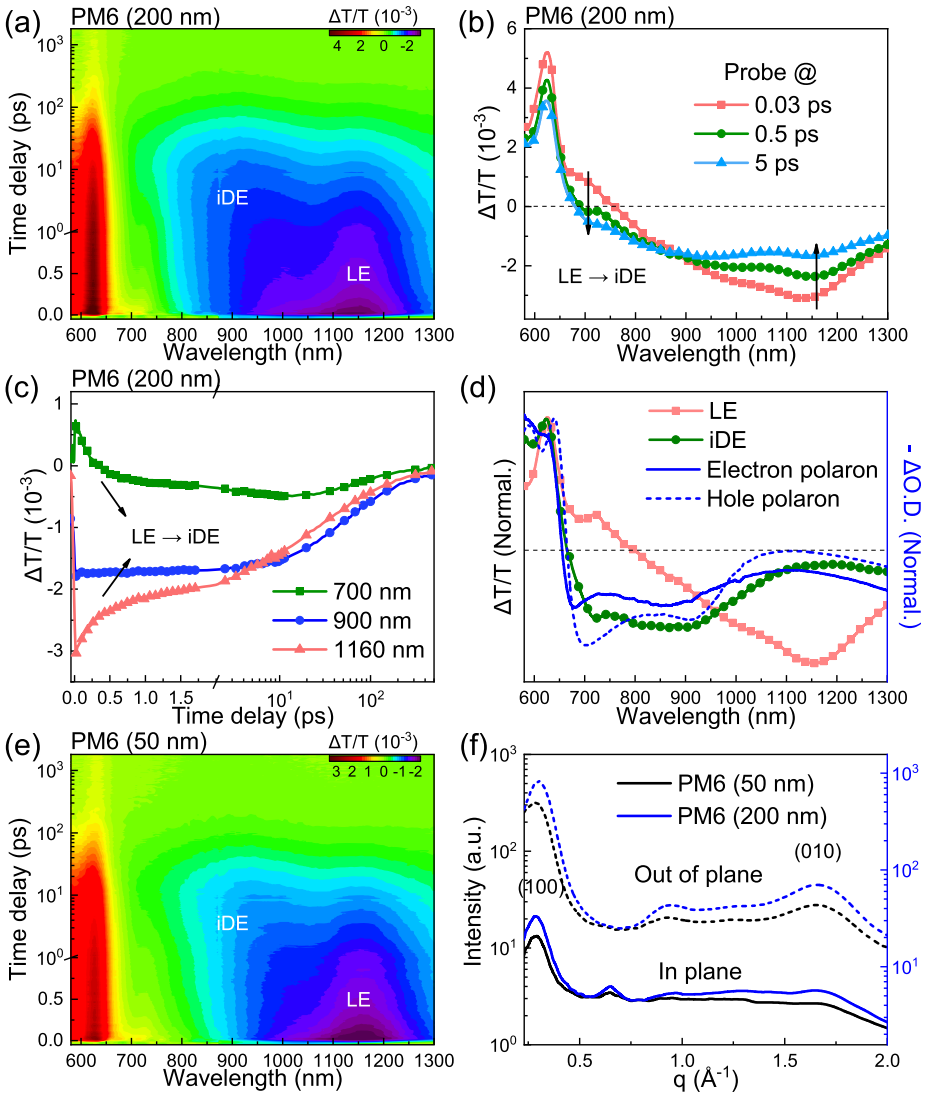

Figure 2. (a) Pseudo-color plot of broadband TA data. (b) TA spectra at different time delays and (c) dynamic traces probed at different wavelengths recorded from a 200 nm thick PM6 film. (d) The spectral characteristics of LE and iDE states in the PM6 film derived from global analysis algorithm are compared with the absorption change induced by electron/hole polarons characterized by the spectro-electrochemistry measurements. (e) Broadband TA data recorded from a 50 nm thick PM6 film. (f) The profiles of line cuts of GIWAXS data recorded from the PM6 films with thicknesses of 200 and 50 nm, respectively. TA data were recorded with a pump wavelength at 600 nm.

process in NFA-based OPV blends.[9,22−24] Such a scenario is inefficient for describing charge generation from excitations distant from the interface in device structures with large domain sizes. The high-performance donor partners with NFAs are semiconducting copolymers made of electron donating (D) and accepting (A) units.[9,25−28] With limited exciton diffusion lengths in polymer donors,[1,29] the efficient charge generation from the excitations distant from the interface cannot be ascribed to the xCT-mediated channel. The scenario of long-range charge separation has been proposed and identified in polymer/fullerene blends.[30−32] The spatial extent of such a dissociation process for Frenkel excitons in polymers is less than 10 nm in typical polymer/fullerene blends,[31] which is too short to account for the distant excitations in pseudo-PHJ structures.

To elucidate the mechanism of charge separation from excitations distant from interfaces, we probe the excited-state dynamics in pseudo-PHJ and BHJ structures of polymer donor PM6 and NFA Y6 using broadband transient absorption (TA) spectroscopy. The domain sizes are controlled by the donor thickness in pseudo-PHJs and the donor:acceptor weight ratio in BHJs. In addition to the xCT state, we observe a new intermediate state of intra-moiety delocalized excitations (iDEs) for electron transfer channels in the samples with large domain sizes (Figure 1d). The iDE-mediated channel is a long-range charge separation pathway, probably responsible for the thickness tolerance and device structure compatibility in NFA-based OPV devices.

The model system of polymer donor PM6 and NFA Y6 studied in this work show excellent performances in devices with both BHJ and pseudo-PHJ device structures.[17,33] With increasing the active layer thickness, the PCEs are largely retained, suggesting efficient charge generation from excitations distant from the donor:acceptor interface.[19] In order to identify the excited-state dynamics associated with the excitations next to and distant from the interfaces, we prepare the neat polymer film, the BHJ, and the pseudo-PHJ structures with different donor domain sizes (see Experimental Section

https://doi.org/10.1021/acs.jpclett.3c01861
J. Phys. Chem. Lett. 2023, 14, 7498−7506

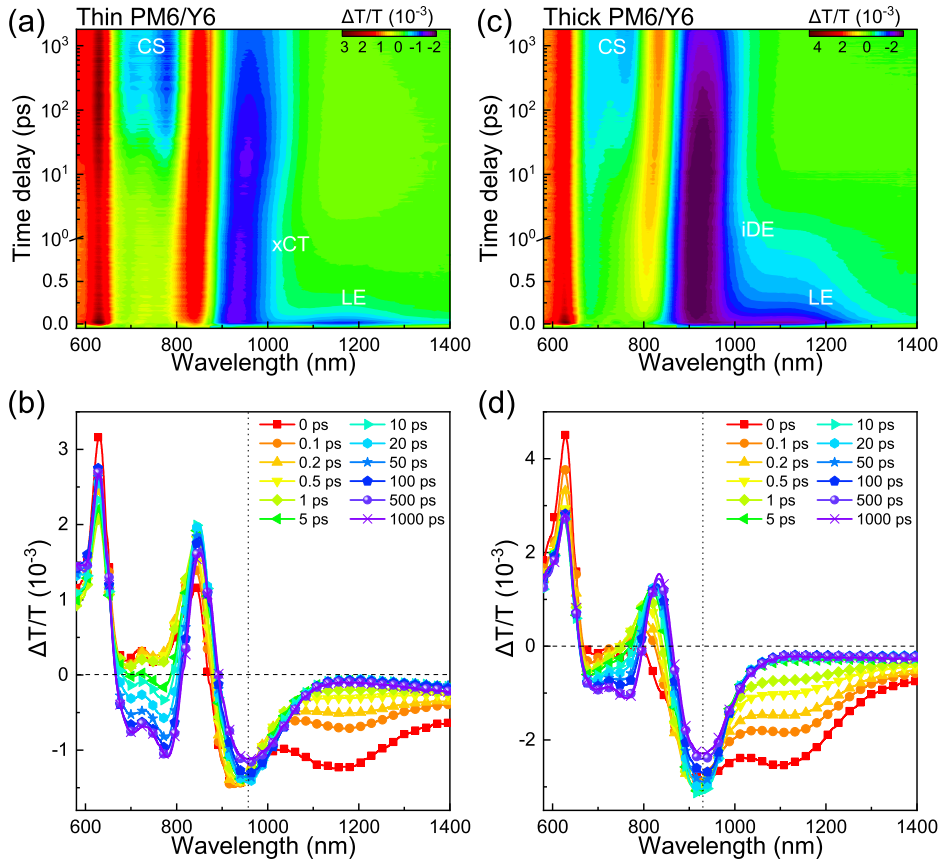

Figure 3. Pseudo-color plots of broadband TA data and TA spectra at different time delays recorded from pseudo-PHJs with (a, b) 50 nm thick and (c, d) 200 nm thick PM6 layers, respectively.

and Figure S1 for details). In brief, the neat films with thicknesses of ∼50 nm and ∼200 nm, hereafter referred to as thin and thick samples, are prepared on silica substrates by controlling the solution concentration. The NFA Y6 dissolved in an orthogonal solvent is then sequentially deposited on these PM6 films to fabricate the pseudo-PHJ structures.[34] Due to certain miscibility, the pseudo-PHJ structure prepared on the thin layer of the polymer donor is formed with relatively small domain sizes. In contrast, the domain size in the pseudo-PHJ sample prepared on the thick layer of PM6 is possibly larger than the exciton diffusion length. For BHJ structures, the mixed donor and acceptor with optimal weight ratios (1:1.2) and donor-enriched ratios (1:0.2) in solutions are deposited on the substrates. The domain size of the polymer donor is much larger in the donor-enriched BHJ sample. The differences between the excited-state dynamics in the samples with different domain sizes are probed with broadband TA spectroscopy with a temporal resolution better than ∼20 fs (Figure S2).

In the well-mixed PM6:Y6 blend films, electron transfer occurs on an ultrafast time scale. Most of the optically induced local excitations (LEs) are converted into the xCT state on a time scale of ∼0.15 ps.[23,24] In the samples with large donor domains, charge transfer from excitations in polymer donors is much slower so that the excited-state evolution on a later time scale in neat PM6 films may become important.

Figure 2a shows broadband TA data recorded from thick film PM6. Simultaneously upon pulse pumping, we observe a ground-state bleaching (GSB) band centered at ∼625 nm, a stimulated emission (SE) band centered at ∼700 nm, and an excited-state absorption (ESA) band centered at ∼1160 nm, respectively. On the subpicosecond time scale, a spectral transfer is prominent with the ESA band shift to the shorter wavelength range centered at 900 nm (Figure 2b). The early stage lifetime is ∼0.3 ps, which is also manifested on the dynamics of SE feature (Figure 2c). These results suggest an ultrafast conversion of photon-induced LEs to a new excited species. Using the global fitting analysis, we can estimate that ∼65% of the primary excitations are converted into the new species (Figure S3). The lifetime of new excited species increases to ∼130 ps from ∼34 ps for the residual LEs (Figure S3), which may make substantial contributions to charge generation.

In D−A copolymers, multiple configurations of excited states may be optically excited arising from different local electronic interactions in chromophore complexes.[2,35−42] To gain more insights about the newly generated excited species, we compare the characteristic spectra with the spectral features of polarons identified by spectro-electrochemistry measurements (Figure 2d).[38,41] The spectral profile of the new excited species is comparable to that of charged polarons, suggesting that the spatial distributions of the electron and hole in it are not fully overlapped. On the other hand, the recombination dynamics are largely independent of excitation density (Figure S4), which is different from bimolecular recombination expected for free charges. Such a bound state with partially separated electron and hole is similar to the state of polaron pairs (sometimes referred to as spatially indirect or charge-transfer excitons) as discussed in the literature.[35−41] The spatial extent of such a partially separated state of electron−

https://doi.org/10.1021/acs.jpclett.3c01861
J. Phys. Chem. Lett. 2023, 14, 7498−7506

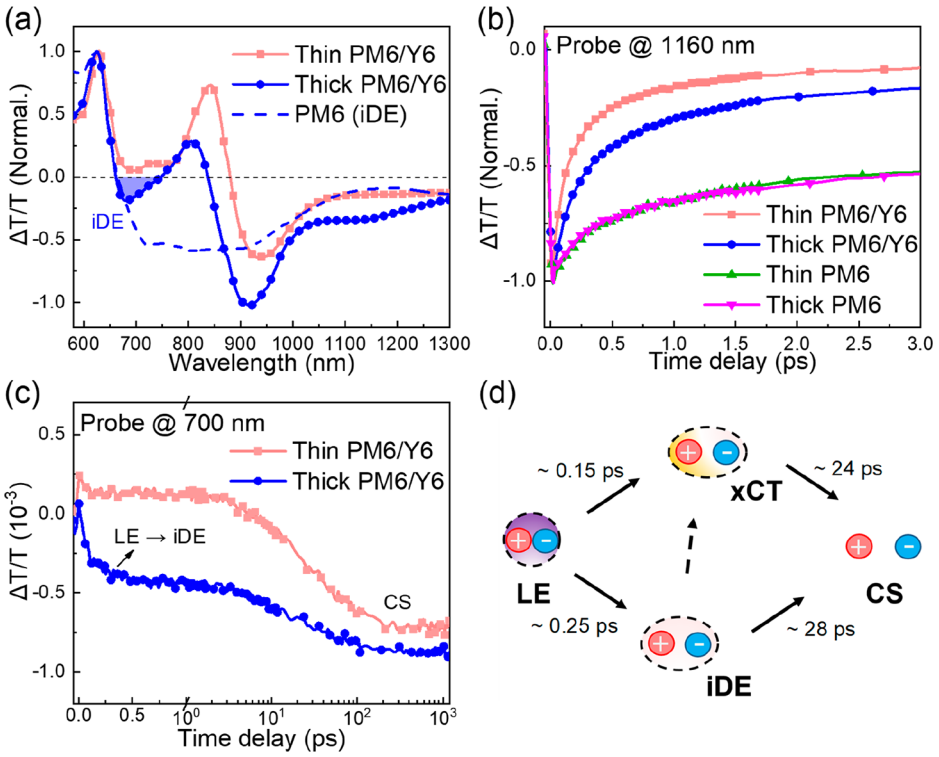

Figure 4. (a) Normalized spectra of intermediate states from thin and thick pseudo-PHJ films recorded at a time delay of 0.5 ps. The spectrum of the iDE state in the neat PM6 film is also shown for comparison. Normalized TA dynamics probed at (b) 1160 nm and (c) TA dynamics probed at 700 nm recorded from the pseudo-PHJs with thin and thick PM6 layers. (d) Schematics of the excited states and dynamic processes involved in the charge generation in pseudo-PHJs.

hole pairs is susceptible to the interchromophore interactions in polymers, which may be created in either intrachain or interchain configurations. We quote such an excited state with the wave function delocalized over multiple chromophore units in the polymer domain as an intra-moiety delocalized excitation (iDE), while the LE generally refers to Frenkel-type excitations in which the electron and hole wave functions are distributed on the same chromophore.

The electronic configuration of an iDE state is primarily determined by short-range charge-transfer and long-range dipole−dipole interactions in the chromophore complex, which is susceptible to the local morphology aspects such as molecular orientations, stacking geometries, and crystalline structures. The formation of such an iDE state is dependent on the sample thickness (Figure 2e). In the thin sample, the ratio of LE converted into the iDE state is reduced to ∼45% (Figure S3), which is probably caused by the different molecular aggregation in the samples. The grazing incidence wide-angle X-ray scattering (GIWAXS) results (Figure 2f and Figure S5) show that the (010) peak in the out-of-plane direction and the (100) peak in the in-plane direction are more distinct in the thick sample. In comparison with the thin sample, the molecular stacking distance is shorter and the coherent crystalline length is longer in the thick sample (Figure S5).[43,44] The formation of iDE is promoted by the enhanced interchromophore interaction in the thick sample with tight packing and high crystallinity. The correlation between iDE formation and polymer aggregation is further confirmed by the experiments in solution samples. In the heated solution, the polymer aggregation is largely reduced, which, in turn, significantly suppresses the formation of iDE states (Figure S6). Since the lifetime of the iDE is longer than that of LE, and the delocalization property of iDE caused by the interchromophore interaction is helpful to increasing hopping length, the iDE should make more important contributions than the LE in thick samples with large domain sizes.[45−48]

We probe the excited-state dynamics in the pseudo-PHJ structures with thin and thick donor layers to disentangle the charge separation pathways from excitations adjacent to and distant from the interfaces. The optical pump is from the side of donor PM6 with the pump wavelength resonant to the absorption of PM6 (Figures S1 and S2). Considering the penetration depth of <100 nm for polymer PM6 film at the incident wavelength (Figure S7), the distances from a large portion of primary excitations to the donor:acceptor interface are longer than the exciton diffusion length in the thick sample. In the thin sample, the excitations are created much closer to the interface, while the penetrated pump light may also excite the acceptor Y6.

Figure 3 compares the TA data recorded from the pseudo-PHJ structures with donor layers of different thicknesses. While the spectral features of the resulted charge-separated states (>100 ps) are similar, the spectral features of the intermediate excited states show significant differences in the two samples (Figure 3a and c). In the thin sample, the spectro-temporal dynamics are similar to that in well-mixed blends.[24] The primary LEs are converted into the xCT states, which dissociate into free charges (Figure 3b). In the thick sample, the LEs are longer-lived with reduced conversion to xCT states (Figure 3d) allowing the formation of iDEs.

We compare the TA spectra obtained at a delay of 0.5 ps from different samples (Figure 4a). The spectrum recorded from the thin sample is mainly contributed by the xCTs and the residual excitations in NFAs. However, in the thick pseudo-

https://doi.org/10.1021/acs.jpclett.3c01861
J. Phys. Chem. Lett. 2023, 14, 7498−7506

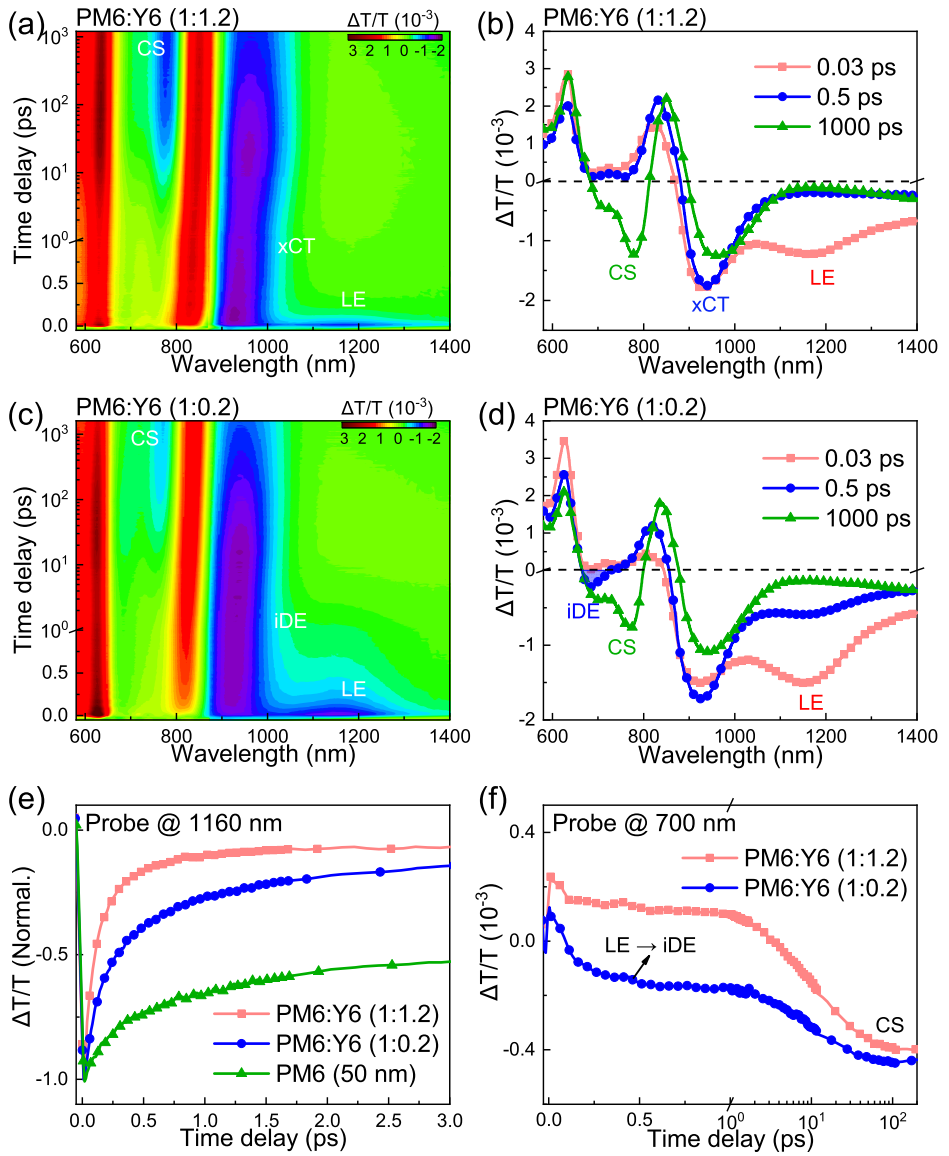

Figure 5. Pseudo-color plots of broadband TA data and TA spectra at different time delays recorded from BHJs with optimized (a, b) and donor enriched (c, d) weight ratios, respectively. (e) Normalized TA dynamics probed at 1160 nm and (f) TA data probed at 700 nm recorded from the BHJs with different D:A weight ratios.

PHJ sample, the spectrum is significantly influenced by iDEs converted from excitations further away from the interfaces. This results in a substantial contribution to the highlighted ESA band in the range of 650−750 nm, which is a characteristic of iDEs. This band is not observed in the thin pseudo-PHJs, where the conversion from LEs to xCTs occurs more quickly near the interfaces.

The effect of domain size is also manifested in the lifetimes of excited-state conversion in the pseudo-PHJ structures. In comparison with the thin pseudo-PHJ sample, the ESA feature of LEs at 1160 nm is longer-lived (Figure 4b) in the thick sample, which allows the formation of iDE states on a longer time scale (Figure 4c). The intermediates of either xCT or iDE states can efficiently dissociate into free charges (Figure 4c). By analyzing the dynamic traces of charge generation with a multiexponential growth function (Figure S8), we estimate that the major lifetimes are ∼24 and ∼28 ps for the charge separation from the xCT and iDE states in the thin and thick pseudo-PHJ structures, respectively. These results indicate the presence of two pathways for charge separation in pseudo-PHJ heterostructures (Figure 4d). In addition to the xCT-mediated channel, the excitations distant from the interfaces may be converted into the iDE states, which further dissociate into free charges. The efficiency is quite high with the relatively longer lifetime of the iDE state. The iDE-mediated electron transfer pathway can well explain the long-range charge separation in the samples with large donor domains. In these samples, the iDE state acts as an important intermediate for charge separation without forming the bound xCT states first, reducing the loss induced by LE recombination during exciton diffusion.

Intuitively, the iDE-mediated channel may be considered as a precursor step for the xCT-mediated channel in a sequential scenario. The iDEs may diffuse through a long-range Förster energy transfer mechanism to form the xCT states first,[49] which, however, is unlikely to be the case here. For the xCT-mediated channel, the ESA feature at ∼900 nm gradually shifts to the longer wavelength side to ∼940 nm (Figure 3b) due to

https://doi.org/10.1021/acs.jpclett.3c01861
J. Phys. Chem. Lett. 2023, 14, 7498−7506

the modified electric field caused by increased electron−hole separation, which strongly modulates the optical response by influencing neighboring molecules as previously discussed in OPV systems.[24,31,50−53] Such a spectral shift is not observed for the iDE-mediated channel (Figure 3d). The ESA feature that emerges at ∼940 nm is similar to the spectral feature of free charges, suggesting that the electron and hole is readily separated upon the conversion from iDEs in the polymer PM6. In other words, most iDEs dissociate into free charges without forming the xCT state, mitigating the energy loss related to the interface.

In the literature, long-range dissociation of Frenkel-type excitons in polymer/fullerene blends was found to be susceptible to the rate of electron transfer induced by short-range interchromophore electronic interaction and the rate of exciton diffusion governed by long-range dipolar interaction.[30,54] In comparison with Frenkel excitations, the iDE state with reduced exciton binding is more favorable for efficient charge separation with a small driving force. In theory, the delocalization effect of excited states may extend the spatial range of charge separation and significantly promotes the effective length of excitation diffusion.[45−48] These effects are possibly responsible for the long-range charge separation from iDEs observed in this work, which deserves a more in-depth study in the future.

Next, we study the role of the iDE channel in the BHJ structures. Figure 5 shows the TA data recorded from the BHJ samples with an optimal donor:acceptor weight ratio (1:1.2) and donor-enriched ratio (1:0.2). In the donor-enriched sample, a larger domain size of the polymer donor is expected so that the iDE-mediate channel may play a more significant role. In the sample with an optimal weight ratio, the xCT state meditated channel dominates the process of charge separation. On the time scale of ∼0.1 ps, LEs created in the polymer domains are converted into xCT states which further dissociate into the CS state (Figure 5a). The ESA feature at ∼900 nm shows a gradual shift to the longer wavelength side during the dissociation of the xCT state (Figure 5b). In the donor-enriched sample, the reduced density of interfacial states allows a certain portion of LEs to be converted into the iDE states (Figure 5c−f), manifested with the ESA feature in the range of 650−750 nm (Figure 5d). The shift of ESA in the range of 900−1000 nm (Figure 5d) in donor-enriched BHJ is less than that in the optimally mixed BHJ, suggesting that two charge separation channels mediated by either the xCT state or the iDE state function in the donor-enriched BHJ. The experimental data well support an important role played by iDEs in the charge generation in BHJ structures with large donor domains.

The iDE-mediated electron transfer channel can explain the device structure compatibility in OPV devices with polymer/NFA blends. In spite of the slower charge separation from the iDE states, the charge generation efficiency largely remains considering the longer-lived nature of the iDE states compared to the LE states. The long-range electron transfer can address the exciton diffusion limitation for excitations distant from the interfaces in polymer donors. In champion OPV devices using copolymer donors and small-molecule NFAs, the channel of hole transfer from the excitations in NFA domains makes substantial contributions to photocharge generation.[24,55] In comparison with fullerene acceptors, the exciton diffusion is more efficient in NFAs, enlarging the spatial extent of hole transfer in NFA-based systems.[19,56−58] The charge separation becomes less sensitive to the domain size, possibly responsible for weak dependence of device performance on annealing temperature in NFA-based devices.[33] Benefiting from the iDE-mediated channel, the diffusion limitation on the domain size is no longer a strict constraint in thick BHJs and pseudo-PHJs, which contributes to the large-scale printing procedure toward commercial applications. In pseudo-PHJ structures with increased domain sizes, the charge separation remains highly efficient. As the interfacial area is significantly reduced in pseudo-PHJs, the xCT-related charge recombination loss channels in the OPV device could be suppressed, such as the triplet loss channel formed by bimolecular recombination at D−A interfaces.[59,60] As a result, the pseudo-PHJ devices with suitable polymer/NFA partners may outperform the BHJ devices.[18]

In PM6, the large conjugation units on backbones promote chain rigidity and $\pi-\pi$ stacking, reducing the entropy of mixing.[25] The clear vibration peaks in the absorption spectra (Figure S1) and regular packing in GIWAXS measurements (Figure S5) of PM6 indicate the regular and conjugated aggregation of PM6 chromophores, which leads to strong electronic coupling and results in the formation of iDEs. The conversion from the LE to iDE is also observed in other representative copolymer donors such as D18 and PTQ10 (Figure S9), which illustrates the broad importance of iDEs for efficient OPVs.[26,61] In such a D−A copolymer, the low-lying excited states are created with combined Frenkel-type local and CT characters. In quality, theoretical treatment with a model Hamiltonian suggests that the spatial extent of such a delocalized state is regulated by the interplay between dipole−dipole interaction, charge-transfer interaction, and exciton-vibration interaction in the chromophore complex.[62,63] The iDE state may be generated coherently from optical excitations or incoherently from optically induced LEs. In the PM6:Y6 system, the formation of iDE is slower than that of the xCT state next to the interface, and the dissociation of iDE is also slower than that of the xCT state, which is reasonable since most available OPV materials are designed for the xCT-mediated channel. In principle, the charge-transfer interaction is sensitive to the wave function overlap, and the dipole−dipole interaction is dependent on the dipole orientation. To improve the spatial extent and generation yield of iDEs, the electron affinity, molecular packing and intermolecular spacing can be manipulated via molecular engineering (e.g., halogen substitution and side chain engineering), ternary mixing, morphology control (e.g., deposition method, additive adding and annealing), etc.[43,64] Possibly, the iDE-mediated channel may be optimized to be as effective as the xCT-mediated channel.

In conclusion, our study has revealed a long-range charge separation pathway mediated by the iDE state in polymer donors, presented in both the PHJ and BHJ structures. This pathway facilitates photocharge generation from excitations created at a distance from the interfaces. Our findings suggest that delocalized excitations can dissociate into free charges of electrons and holes without forming the bound xCT states first. This discovery addresses the limitations associated with exciton diffusion in the design of OPV devices. Moreover, the iDE-mediated pathway not only alleviates the domain size constraints but also suppresses the recombination loss at the interfaces, thus improving the device compatibility of NFA-based devices. In the future, efforts to synergize the long-range iDE and short-range xCT pathways may help to overcome

https://doi.org/10.1021/acs.jpclett.3c01861
J. Phys. Chem. Lett. 2023, 14, 7498−7506

some of the persistent shortcomings in OPV devices, narrowing the power conversion efficiency gap between organic and inorganic solar cells.

■ ASSOCIATED CONTENT

Supporting Information

The Supporting Information is available free of charge at https://pubs.acs.org/doi/10.1021/acs.jpclett.3c01861.

Experimental methods for sample preparation; TA spectroscopy measurements and spectro-electrochemical measurements; absorption figures; global analysis results; excitation−density dependent dynamics; GIWAX characterizations; TA characterization of the PM6 solution; estimation of the penetration depth; fitting of temporal dynamics (PDF); iDEs in other copolymers

■ AUTHOR INFORMATION

Corresponding Authors

Min Xiao − *National Laboratory of Solid State Microstructures, School of Physics, and Collaborative Innovation Center for Advanced Microstructures, Nanjing University, Nanjing 210093, China; Department of Physics, University of Arkansas, Fayetteville, Arkansas 72701, United States*; Email: mxiao@uark.edu

Chunfeng Zhang − *National Laboratory of Solid State Microstructures, School of Physics, and Collaborative Innovation Center for Advanced Microstructures, Nanjing University, Nanjing 210093, China; Institute of Materials Engineering, Nanjing University, Nantong, Jiangsu 226001, China*; orcid.org/0000-0001-9030-5606; Email: cfzhang@nju.edu.cn

Authors

Qian Li − *National Laboratory of Solid State Microstructures, School of Physics, and Collaborative Innovation Center for Advanced Microstructures, Nanjing University, Nanjing 210093, China*

Rui Wang − *College of Physics, Nanjing University of Aeronautics and Astronautics, Nanjing 211106, China; Key Laboratory of Aerospace Information Materials and Physics (NUAA), MIIT, Nanjing 211106, China*

Tao Yu − *National Laboratory of Solid State Microstructures, School of Physics, and Collaborative Innovation Center for Advanced Microstructures, Nanjing University, Nanjing 210093, China*; orcid.org/0000-0003-1981-3469

Xiaoyong Wang − *National Laboratory of Solid State Microstructures, School of Physics, and Collaborative Innovation Center for Advanced Microstructures, Nanjing University, Nanjing 210093, China*; orcid.org/0000-0003-1147-0051

Zhi-Guo Zhang − *State Key Laboratory of Organic/Inorganic Composites, Beijing Advanced Innovation Center for Soft Matter Science and Engineering, Beijing University of Chemical Technology, Beijing 100029, China*; orcid.org/0000-0003-4341-7773

Yuan Zhang − *School of Chemistry, Beijing Advanced Innovation Center for Biomedical Engineering, Beihang University, Beijing 100191, China*; orcid.org/0000-0003-0670-2428

Complete contact information is available at: https://pubs.acs.org/10.1021/acs.jpclett.3c01861

Notes

The authors declare no competing financial interest.

■ ACKNOWLEDGMENTS

This work is supported by the National Key R&D Program of China (Grant Nos. 2022YFB3206900 and 2018YFA0209101), the National Science Foundation of China (Grant NOs. 22225305, 21922302, and 21873047), the People's Livelihood Project of Nantong City (MS22022066), and the Fundamental Research Funds for the Central University. The authors acknowledge Dr. Xuewei Wu for providing technical assistance.

■ REFERENCES

(1) Clarke, T. M.; Durrant, J. R. Charge Photogeneration in Organic Solar Cells. *Chem. Rev.* **2010**, *110* (11), 6736−6767.

(2) Dimitriev, O. P. Dynamics of Excitons in Conjugated Molecules and Organic Semiconductor Systems. *Chem. Rev.* **2022**, *122* (9), 8487−8593.

(3) Bakulin, A. A.; Rao, A.; Pavelyev, V. G.; van Loosdrecht, P. H. M.; Pshenichnikov, M. S.; Niedzialek, D.; Cornil, J.; Beljonne, D.; Friend, R. H. The Role of Driving Energy and Delocalized States for Charge Separation in Organic Semiconductors. *Science* **2012**, *335* (6074), 1340−1344.

(4) Coropceanu, V.; Chen, X.-K.; Wang, T.; Zheng, Z.; Brédas, J. L. Charge-Transfer eEectronic States in Organic Solar Cells. *Nat. Rev. Mater.* **2019**, *4* (11), 689−707.

(5) Xu, Z.; Zhou, Y.; Yam, C. Y.; Groß, L.; De Sio, A.; Frauenheim, T.; Lienau, C.; Chen, G. Revealing Generation, Migration, and Dissociation of Electron-Hole Pairs and Current Emergence in an Organic Photovoltaic Cell. *Sci. Adv.* **2021**, *7* (25), No. eabf7672.

(6) Mikhnenko, O. V.; Blom, P. W. M.; Nguyen, T.-Q. Exciton Diffusion in Organic Semiconductors. *Energy Environ. Sci.* **2015**, *8* (7), 1867−1888.

(7) Tang, C. W. Two-Layer Organic Photovoltaic Cell. *Appl. Phys. Lett.* **1986**, *48* (2), 183−185.

(8) Yu, G.; Gao, J.; Hummelen, J. C.; Wudl, F.; Heeger, A. J. Polymer Photovoltaic Cells: Enhanced Efficiencies via a Network of Internal Donor-Acceptor Heterojunctions. *Science* **1995**, *270* (5243), 1789−1791.

(9) Zhang, G.; Lin, F. R.; Qi, F.; Heumuller, T.; Distler, A.; Egelhaaf, H. J.; Li, N.; Chow, P. C. Y.; Brabec, C. J.; Jen, A. K.; et al. Renewed Prospects for Organic Photovoltaics. *Chem. Rev.* **2022**, *122* (18), 14180−14274.

(10) Zhang, Y.; Wu, B.; He, Y.; Deng, W.; Li, J.; Li, J.; Qiao, N.; Xing, Y.; Yuan, X.; Li, N.; et al. Layer-by-Layer Processed Binary All-Polymer Solar Cells with Efficiency over 16% Enabled by Finely Optimized Morphology. *Nano Energy* **2022**, *93*, 106858.

(11) Park, S. Y.; Labanti, C.; Luke, J.; Chin, Y. C.; Kim, J. S. Organic Bilayer Photovoltaics for Efficient Indoor Light Harvesting. *Adv. Energy Mater.* **2022**, *12* (3), 2103237.

(12) Sun, R.; Wang, T.; Yang, X.; Wu, Y.; Wang, Y.; Wu, Q.; Zhang, M.; Brabec, C. J.; Li, Y.; Min, J. High-Speed Sequential Deposition of Photoactive Layers for Organic Solar Cell Manufacturing. *Nat. Energy* **2022**, *7* (11), 1087−1099.

(13) Liu, S.; Li, H.; Wu, X.; Chen, D.; Zhang, L.; Meng, X.; Tan, L.; Hu, X.; Chen, Y. Pseudo-Planar Heterojunction Organic Photovoltaics with Optimized Light Utilization for Printable Solar Windows. *Adv. Mater.* **2022**, *34* (23), No. 2201604.

(14) Sun, R.; Guo, J.; Wu, Q.; Zhang, Z.; Yang, W.; Guo, J.; Shi, M.; Zhang, Y.; Kahmann, S.; Ye, L.; et al. A Multi-Objective Optimization-Based Layer-by-Layer Blade-Coating Approach for Organic Solar Cells: Rational Control of Vertical Stratification for High Performance. *Energy Environ. Sci.* **2019**, *12* (10), 3118−3132.

(15) Ghasemi, M.; Ye, L.; Zhang, Q.; Yan, L.; Kim, J.-H.; Awartani, O.; You, W.; Gadisa, A.; Ade, H. Panchromatic Sequentially Cast Ternary Polymer Solar Cells. *Adv. Mater.* **2017**, *29* (4), 1604603.

(16) Ye, L.; Xiong, Y.; Chen, Z.; Zhang, Q.; Fei, Z.; Henry, R.; Heeney, M.; O'Connor, B. T.; You, W.; Ade, H. Sequential

Deposition of Organic Films with Eco-Compatible Solvents Improves Performance and Enables over 12%-Efficiency Nonfullerene Solar Cells. *Adv. Mater.* **2019**, *31* (17), No. 1808153.
(17) Jiang, K.; Zhang, J.; Peng, Z.; Lin, F.; Wu, S.; Li, Z.; Chen, Y.; Yan, H.; Ade, H.; Zhu, Z.; Jen, A. K.-Y. Pseudo-Bilayer Architecture Enables High-Performance Organic Solar Cells with Enhanced Exciton Diffusion Length. *Nat. Commun.* **2021**, *12* (1), 468.
(18) Jiang, K.; Zhang, J.; Zhong, C.; Lin, F. R.; Qi, F.; Li, Q.; Peng, Z.; Kaminsky, W.; Jang, S.-H.; Yu, J.; et al. Suppressed Recombination Loss in Organic Photovoltaics Adopting a Planar−Mixed Heterojunction Architecture. *Nat. Energy* **2022**, *7* (11), 1076−1086.
(19) Cai, Y.; Li, Q.; Lu, G.; Ryu, H. S.; Li, Y.; Jin, H.; Chen, Z.; Tang, Z.; Lu, G.; Hao, X.; Woo, H. Y.; Zhang, C.; Sun, Y. Vertically Optimized Phase Separation with Improved Exciton Diffusion Enables Efficient Organic Solar Cells with Thick Active Layers. *Nat. Commun.* **2022**, *13* (1), 2369.
(20) Ma, L.; Zhang, S.; Yao, H.; Xu, Y.; Wang, J.; Zu, Y.; Hou, J. High-Efficiency Nonfullerene Organic Solar Cells Enabled by 1000 nm Thick Active Layers with a Low Trap-State Density. *ACS Appl. Mater. Interfaces* **2020**, *12* (16), 18777−18784.
(21) Ma, L.; Xu, Y.; Zu, Y.; Liao, Q.; Xu, B.; An, C.; Zhang, S.; Hou, J. A Ternary Organic Solar Cell with 300 nm Thick Active Layer Shows Over 14% Efficiency. *Sci. China: Chem.* **2020**, *63* (1), 21−27.
(22) Hinrichsen, T. F.; Chan, C. C. S.; Ma, C.; Palecek, D.; Gillett, A.; Chen, S.; Zou, X.; Zhang, G.; Yip, H.-L.; Wong, K. S.; Friend, R. H.; Yan, H.; Rao, A.; Chow, P. C. Y. Long-Lived and Disorder-Free Charge Transfer States Enable Endothermic Charge Separation in Efficient Non-Fullerene Organic Solar Cells. *Nat. Commun.* **2020**, *11* (1), 5617.
(23) Wu, J.; Lee, J.; Chin, Y.-C.; Yao, H.; Cha, H.; Luke, J.; Hou, J.; Kim, J.-S.; Durrant, J. R. Exceptionally Low Charge Trapping Enables Highly Efficient Organic Bulk Heterojunction Solar Cells. *Energy Environ. Sci.* **2020**, *13* (8), 2422−2430.
(24) Wang, R.; Zhang, C.; Li, Q.; Zhang, Z.; Wang, X.; Xiao, M. Charge Separation from an Intra-Moiety Intermediate State in The High-Performance PM6:Y6 Organic Photovoltaic Blend. *J. Am. Chem. Soc.* **2020**, *142* (29), 12751−12759.
(25) Zheng, Z.; Yao, H.; Ye, L.; Xu, Y.; Zhang, S.; Hou, J. PBDB-T and Its Derivatives: A family of Polymer Donors Enables over 17% Efficiency in Organic Photovoltaics. *Mater. Today* **2020**, *35*, 115−130.
(26) Liu, Q.; Jiang, Y.; Jin, K.; Qin, J.; Xu, J.; Li, W.; Xiong, J.; Liu, J.; Xiao, Z.; Sun, K.; et al. 18% Efficiency Organic Solar Cells. *Sci. Bull.* **2020**, *65* (4), 272−275.
(27) Li, X.; Pan, F.; Sun, C.; Zhang, M.; Wang, Z.; Du, J.; Wang, J.; Xiao, M.; Xue, L.; Zhang, Z.-G.; Zhang, C.; Liu, F.; Li, Y. Simplified Synthetic Routes for Low Cost and High Photovoltaic Performance n-Type Organic Semiconductor Acceptors. *Nat. Commun.* **2019**, *10* (1), 519.
(28) Qian, D.; Ye, L.; Zhang, M.; Liang, Y.; Li, L.; Huang, Y.; Guo, X.; Zhang, S.; Tan, Z. a.; Hou, J. Design, Application, and Morphology Study of a New Photovoltaic Polymer with Strong Aggregation in Solution State. *Macromolecules* **2012**, *45* (24), 9611.
(29) Riley, D. B.; Sandberg, O. J.; Li, W.; Meredith, P.; Armin, A. Quasi-Steady-State Measurement of Exciton Diffusion Lengths in Organic Semiconductors. *Phys. Rev. Appl.* **2022**, *17* (2), 024076.
(30) Caruso, D.; Troisi, A. Long-Range Exciton Dissociation in Organic Solar Cells. *Proc. Natl. Acad. Sci. U. S. A.* **2012**, *109* (34), 13498−13502.
(31) Gélinas, S.; Rao, A.; Kumar, A.; Smith, S. L.; Chin, A. W.; Clark, J.; van der Poll, T. S.; Bazan, G. C.; Friend, R. H. Ultrafast Long-Range Charge Separation in Organic Semiconductor Photovoltaic Diodes. *Science* **2014**, *343* (6170), 512−516.
(32) Falke, S. M.; Rozzi, C. A.; Brida, D.; Maiuri, M.; Amato, M.; Sommer, E.; De Sio, A.; Rubio, A.; Cerullo, G.; Molinari, E.; Lienau, C. Coherent Ultrafast Charge Transfer in an Organic Photovoltaic Blend. *Science* **2014**, *344* (6187), 1001−1005.
(33) Yuan, J.; Zhang, Y.; Zhou, L.; Zhang, G.; Yip, H.-L.; Lau, T. K.; Lu, X.; Zhu, C.; Peng, H.; Johnson, P. A.; et al. Single-Junction Organic Solar Cell with Over 15% Efficiency Using Fused-Ring Acceptor with Electron-Deficient Core. *Joule* **2019**, *3* (4), 1140−1151.
(34) Wan, J.; Zeng, L.; Liao, X.; Chen, Z.; Liu, S.; Zhu, P.; Zhu, H.; Chen, Y. All-Green Solvent-Processed Planar Heterojunction Organic Solar Cells with Outstanding Power Conversion Efficiency of 16. *Adv. Funct. Mater.* **2022**, *32* (5), 2107567.
(35) Reid, O. G.; Pensack, R. D.; Song, Y.; Scholes, G. D.; Rumbles, G. Charge Photogeneration in Neat Conjugated Polymers. *Chem. Mater.* **2014**, *26* (1), 561−575.
(36) Rolczynski, B. S.; Szarko, J. M.; Son, H. J.; Liang, Y.; Yu, L.; Chen, L. X. Ultrafast Intramolecular Exciton Splitting Dynamics in Isolated Low-Band-Gap Polymers and Their Implications in Photovoltaic Materials Design. *J. Am. Chem. Soc.* **2012**, *134* (9), 4142.
(37) Tautz, R.; Da Como, E.; Wiebeler, C.; Soavi, G.; Dumsch, I.; Frohlich, N.; Grancini, G.; Allard, S.; Scherf, U.; Cerullo, G.; et al. Charge Photogeneration in Donor-Acceptor Conjugated Materials: Influence of Excess Excitation Energy and Chain Length. *J. Am. Chem. Soc.* **2013**, *135* (11), 4282−4290.
(38) Di Nuzzo, D.; Viola, D.; Fischer, F. S.; Cerullo, G.; Ludwigs, S.; Da Como, E. Enhanced Photogeneration of Polaron Pairs in Neat Semicrystalline Donor-Acceptor Copolymer Films via Direct Excitation of Interchain Aggregates. *J. Phys. Chem. Lett.* **2015**, *6* (7), 1196−1203.
(39) De Sio, A.; Troiani, F.; Maiuri, M.; Rehault, J.; Sommer, E.; Lim, J.; Huelga, S. F.; Plenio, M. B.; Rozzi, C. A.; Cerullo, G.; Molinari, E.; Lienau, C.; et al. Tracking the Coherent Generation of Polaron Pairs in Conjugated Polymers. *Nat. Commun.* **2016**, *7*, 13742.
(40) Tautz, R.; Da Como, E.; Limmer, T.; Feldmann, J.; Egelhaaf, H.-J.; von Hauff, E.; Lemaur, V.; Beljonne, D.; Yilmaz, S.; Dumsch, I.; Allard, S.; Scherf, U. Structural Correlations in the Generation of Polaron Pairs in Low-Bandgap Polymers for Photovoltaics. *Nat. Commun.* **2012**, *3*, 970.
(41) Wang, R.; Yao, Y.; Zhang, C.; Zhang, Y.; Bin, H.; Xue, L.; Zhang, Z.-G.; Xie, X.; Ma, H.; Wang, X.; Li, Y.; Xiao, M. Ultrafast Hole Transfer Mediated by Polaron Pairs in All-Polymer Photovoltaic Blends. *Nat. Commun.* **2019**, *10* (1), 398.
(42) Wang, K.; Chen, H.; Zhang, J.; Zou, Y.; Yang, Y. Intrachain and Interchain Exciton-Exciton Annihilation in Donor-Acceptor Copolymers. *J. Phys. Chem. Lett.* **2021**, *12* (16), 3928−3933.
(43) Rivnay, J.; Mannsfeld, S. C. B.; Miller, C. E.; Salleo, A.; Toney, M. F. Quantitative Determination of Organic Semiconductor Microstructure from the Molecular to Device Scale. *Chem. Rev.* **2012**, *112* (10), 5488−5519.
(44) Smilgies, D.-M. Scherrer Grain-Size Analysis Adapted to Grazing-Incidence Scattering with Area Detectors. *J. Appl. Crystallogr.* **2009**, *42* (6), 1030−1034.
(45) Sneyd, A. J.; Beljonne, D.; Rao, A. A New Frontier in Exciton Transport: Transient Delocalization. *J. Phys. Chem. Lett.* **2022**, *13* (29), 6820−6830.
(46) Zhang, G.; Chen, X.-K.; Xiao, J.; Chow, P. C. Y.; Ren, M.; Kupgan, G.; Jiao, X.; Chan, C. C. S.; Du, X.; Xia, R.; Chen, Z.; Yuan, J.; Zhang, Y.; Zhang, S.; Liu, Y.; Zou, Y.; Yan, H.; Wong, K. S.; Coropceanu, V.; Li, N.; Brabec, C. J.; Bredas, J.-L.; Yip, H.-L.; Cao, Y. Delocalization of Exciton and Electron Wavefunction in Non-Fullerene Acceptor Molecules Enables Efficient Organic Solar Cells. *Nat. Commun.* **2020**, *11* (1), 3943.
(47) Jin, X.-H.; Price, M. B.; Finnegan, J. R.; Boott, C. E.; Richter, J. M.; Rao, A.; Menke, S. M.; Friend, R. H.; Whittell, G. R.; Manners, I. Long-range Exciton Transport in Conjugated Polymer Nanofibers Prepared by Seeded Growth. *Science* **2018**, *360* (6391), 897−900.
(48) Wan, Y.; Stradomska, A.; Knoester, J.; Huang, L. Direct imaging of exciton transport in tubular porphyrin aggregates by ultrafast microscopy. *J. Am. Chem. Soc.* **2017**, *139* (21), 7287−7293.
(49) Chen, X.-K.; Qian, D.; Wang, Y.; Kirchartz, T.; Tress, W.; Yao, H.; Yuan, J.; Hülsbeck, M.; Zhang, M.; Zou, Y.; et al. A Unified Description of Non-Radiative Voltage Losses in Organic Solar Cells. *Nat. Energy* **2021**, *6* (8), 799−806.
(50) Menke, S. M.; Cheminal, A.; Conaghan, P.; Ran, N. A.; Greehnam, N. C.; Bazan, G. C.; Nguyen, T.-Q.; Rao, A.; Friend, R. H.

https://doi.org/10.1021/acs.jpclett.3c01861
J. Phys. Chem. Lett. 2023, 14, 7498−7506

Order Enables Efficient Electron-Hole Separation at an Organic Heterojunction with a Amall Energy Loss. *Nat. Commun.* **2018**, *9* (1), 277.
(51) Jakowetz, A. C.; Böhm, M. L.; Sadhanala, A.; Huettner, S.; Rao, A.; Friend, R. H. Visualizing Excitations at Buried Heterojunctions in Organic Semiconductor Blends. *Nat. Mater.* **2017**, *16* (5), 551−557.
(52) Wang, X.; Zeng, R.; Lu, H.; Ran, G.; Zhang, A.; Chen, Y.-N.; Liu, Y.; Liu, F.; Zhang, W.; Tang, Z.; et al. A Simple Nonfused Ring Electron Acceptor with a Power Conversion Efficiency over 16%. *Chin. J. Chem.* **2023**, *41* (6), 665−671.
(53) Xu, Y.; Wang, J.; Yao, H.; Bi, P.; Zhang, T.; Xu, J.; Hou, J. An Asymmetric Non-Fullerene Acceptor with Low Energy Loss and High Photovoltaic Efficiency. *Chin. J. Chem.* **2023**, *41* (9), 1045−1050.
(54) Sneyd, A. J.; Fukui, T.; Palecek, D.; Prodhan, S.; Wagner, I.; Zhang, Y.; Sung, J.; Collins, S. M.; Slater, T. J. A.; Andaji-Garmaroudi, Z.; MacFarlane, L. R.; Garcia-Hernandez, J. D.; Wang, L.; Whittell, G. R.; Hodgkiss, J. M.; Chen, K.; Beljonne, D.; Manners, I.; Friend, R. H.; Rao, A. Efficient Energy Transport in an Organic Semiconductor Mediated by Transient Exciton Delocalization. *Sci. Adv.* **2021**, *7* (32), No. eabh4232.
(55) Stoltzfus, D. M.; Donaghey, J. E.; Armin, A.; Shaw, P. E.; Burn, P. L.; Meredith, P. Charge Generation Pathways in Organic Solar Cells: Assessing the Contribution from the Electron Acceptor. *Chem. Rev.* **2016**, *116* (21), 12920−12955.
(56) Chandrabose, S.; Chen, K.; Barker, A. J.; Sutton, J. J.; Prasad, S. K. K.; Zhu, J.; Zhou, J.; Gordon, K. C.; Xie, Z.; Zhan, X.; et al. High Exciton Diffusion Coefficients in Fused Ring Electron Acceptor Films. *J. Am. Chem. Soc.* **2019**, *141* (17), 6922−6929.
(57) Hume, P. A.; Jiao, W.; Hodgkiss, J. M. Long-Range Exciton Diffusion in a Non-Fullerene Acceptor: Approaching the Incoherent Limit. *J. Mater. Chem. C* **2021**, *9* (4), 1419−1428.
(58) Firdaus, Y.; Le Corre, V. M.; Karuthedath, S.; Liu, W.; Markina, A.; Huang, W.; Chattopadhyay, S.; Nahid, M. M.; Nugraha, M. I.; Lin, Y.; Seitkhan, A.; Basu, A.; Zhang, W.; McCulloch, I.; Ade, H.; Labram, J.; Laquai, F.; Andrienko, D.; Koster, L. J. A.; Anthopoulos, T. D. Long-Range Exciton Diffusion in Molecular Non-Fullerene Acceptors. *Nat. Commun.* **2020**, *11* (1), 5220.
(59) Gillett, A. J.; Privitera, A.; Dilmurat, R.; Karki, A.; Qian, D.; Pershin, A.; Londi, G.; Myers, W. K.; Lee, J.; Yuan, J.; et al. The Role of Charge Recombination to Triplet Excitons in Organic Solar Cells. *Nature* **2021**, *597* (7878), 666−671.
(60) Wang, R.; Xu, J.; Fu, L.; Zhang, C.; Li, Q.; Yao, J.; Li, X.; Sun, C.; Zhang, Z.-G.; Wang, X.; et al. Nonradiative Triplet Loss Suppressed in Organic Photovoltaic Blends with Fluoridated Nonfullerene Acceptors. *J. Am. Chem. Soc.* **2021**, *143* (11), 4359−4366.
(61) Sun, C.; Pan, F.; Bin, H.; Zhang, J.; Xue, L.; Qiu, B.; Wei, Z.; Zhang, Z.-G.; Li, Y. A low Cost and High Performance Polymer Donor Material for Polymer Solar Cells. *Nat. Commun.* **2018**, *9* (1), 743.
(62) Hestand, N. J.; Kazantsev, R. V.; Weingarten, A. S.; Palmer, L. C.; Stupp, S. I.; Spano, F. C. Extended-Charge-Transfer Excitons in Crystalline Supramolecular Photocatalytic Scaffolds. *J. Am. Chem. Soc.* **2016**, *138* (36), 11762−11774.
(63) Hestand, N. J.; Spano, F. C. Expanded Theory of H- and J-Molecular Aggregates: The Effects of Vibronic Coupling and Intermolecular Charge Transfer. *Chem. Rev.* **2018**, *118* (15), 7069−7163.
(64) Sun, W.; Zheng, Y.; Yang, K.; Zhang, Q.; Shah, A. A.; Wu, Z.; Sun, Y.; Feng, L.; Chen, D.; Xiao, Z.; Lu, S.; Li, Y.; Sun, K. Machine Learning-Assisted Molecular Design and Efficiency Prediction for High-Performance Organic Photovoltaic Materials. *Sci. Adv.* **2019**, *5* (11), No. eaay4275.

https://doi.org/10.1021/acs.jpclett.3c01861
J. Phys. Chem. Lett. 2023, 14, 7498−7506